Version: 08/03/11 10:06

Early Weichselian palaeoenvironments reconstructed from a mega-scale thrust-fault complex, Kanin Peninsula, NW Russia

EILIV LARSEN, KURT H. KJÆR, MARIA JENSEN, IGOR N. DEMIDOV, LENA HÅKANSSON AND AAGE PAUS

Larsen, E., Kjær, K.H., Jensen, M., Demidov, I., Håkansson, L. & Paus, Aa.: Early Weichselian palaeoenvironments reconstructed from a mega-scale thrust-fault complex, Kanin Peninsula, NW Russia.

A section, almost 20 km long and up to 80 metres high, through alternating layers of diamict and sorted sediments is superbly exposed on the north coast of the Kanin Peninsula, NW Russia. The diamicts represents multiple glacial advances by the Barents Sea and the Kara Sea ice sheets during the Weichselian. The diamicts and stratigraphically older lacustrine, fluvial and shallow marine sediments have been thrust as nappes by the Barents Sea and Kara Sea ice sheets. Based on stratigraphic position, OSL dating, sea level information, and pollen, it is evident that the sorted sediments were deposited in the Late Eemian – Early Weichselian. Sedimentation started in lake basins and continued in shallow marine embayments when the lakes opened to the sea. The observed transition from lacustrine to shallow marine sedimentation could represent coastal retreat during stable or rising sea level.

Eiliv Larsen (e-mail: eiliv.larsen@ngu.no), Geological Survey of Norway, N-7491 Trondheim, Norway; Kurt H. Kjær, Lena Håkansson, GeoBiosphere Science Centre, Quaternary Sciences, Lund University, Sölvegatan 12, 223 62, Lund, Sweden; Maria Jensen,

Geological Museum, Øster Voldgade 5-7, DK-1350 Copenhagen K, Denmark; Igor N. Demidov, Russian Academy of Sciences, Karelian Research Centre, Institute of Geology, 11 Pushkinskaya Street, Petrozavodsk, 185610 Russia; Aage Paus, Department of Biology, University of Bergen, Allégaten 41, N-5007, Bergen, Norway; 19th April 2004.

In this study, we take advantage of superbly exposed sections on the northern coast of the Kanin Peninsula, northwest Russia to make a detailed reconstruction of sedimentary environments prior to mega-scale glacial dislocation. The latter can be traced over 20-40 kilometres, a feature otherwise only known from marine seismic studies on continental shelves, for instance the Barents shelf to the north of the Kanin peninsula (Sættem 1990; Gataullin *et al.* 2001). Large-scale sedimentary units now occur as discrete interbeds between diamict elements. The uniqueness of the study lies in the combination of different scales that can be applied – from the "marine seismic scale" of dealing with the tectonic nappes (Sættem 1990; Gataullin *et al.* 2001) to the detailed sedimentological analyses of sediment bodies and the characteristics of their bounding surfaces. The developed glacioctonic model, which is a necessary prerequisite for making a reconstruction of the pre-tectonic sedimentary environment, adds important new information for the reconstruction of glaciations in the region during the Weichselian (Svendsen *et al.* 2004), although a more comprehensive discussion of these aspects is given in Kjær *et al.* (this issue) and Larsen *et al.* (this issue).

Glaciotectonic thrusting by glaciers from the Barents and Kara Seas is common from Siberia westwards to the Timan ridge area (Astakhov 2001). The widespread and often complicated nature of the glaciotectonism has not always been recognized. This has led to stratigraphic misinterpretations and a confusing Quaternary stratigraphic nomenclature in northern Russia (Astakhov 2001). Therefore, an additional bonus and again due to the unique continuity of exposure, the study is also well-suited for demonstrating the potential pitfalls

involved when making reconstructions based on poor exposures or from borehole data in areas where glaciotectonics have been operative (Astakhov 2001).

The cliffs on the north coast of the Kanin Peninsula have been investigated previously (Ramsey 1904; Spiridonov & Yakovleva 1961; Lavrushin & Epstein 2001). At the time of the two earliest investigations (Ramsey 1904; Spiridonov & Yakovleva 1961) the coastline must have been situated more than 300 m further offshore than it is today. Nevertheless, the findings are strikingly similar to those of the present study.

Setting

The study area is situated on the northern coast of the Kanin Peninsula (Fig. 1). The northern part of Kanin appears as a plateau ridge. This upland has an average altitude of 150 m a.s.l., reaching a maximum of 241 m, and is a direct continuation of the NW-SE striking Timan Ridge further to the southeast (Fig. 1). From the northern coast of Kanin the terrain rises gently towards the SW. The bedrock topography is smoothened by Quaternary overburden reaching a thickness of at least 80 m, as measured in the exposures. No bedrock is exposed. Diamict sediments crop out on high ground as indicated by scattered erratics. Lacustrine sediments and peat are widespread in the lower areas. Fluvial terraces are found along the rivers. The north coast of Kanin faces the open Barents Sea. High-energy waves, and thawing of the permafrozen sediments cause a rapid cliff retreat giving unique exposure (Fig. 2). Investigations were concentrated along a 20 km-long cliff section between the rivers Madakhá and Krinka (Fig. 1). The cliff is 40 to 80 m high, and dissected by narrow gullies occupied by minor rivers. The section continues both to the east and west for at least another 10 – 20 km.

Methods

Major lithological boundaries were identified on a photo mosaic at a scale approximately 1:600, and used for verifications and corrections in the field. Distances along the coast were measured by GPS with an accuracy of about 5 m. Elevations were measured by a hand-held altimeter (accuracy about 0.5 m) from the high-tide sea level.

The principles of architectural element analyses for sediments (Miall 1988; Boyce & Eyles 2000) were applied. These emphasizes the description of lithological assemblages by defining their bounding surfaces. Recently, this methodology has proved to be an effective tool for understanding the three-dimensional distribution of glacial deposits such as tills and associated sorted sediments. An architectural element can be regarded as a three-dimensional body of genetically related sediment acting as a building block in a stratigraphic succession. Applied to glacial deposits, at least two principal types of architectural elements are defined, diamict elements (DE) and interbeds (I).

Sections along the cliff were logged using a vertical resolution between 1:10 and 1:100. Sorted sediments were divided into sedimentary facies based on grain size, sorting, rounding, and primary sedimentary structures (e.g. Eyles *et al.* 1983). Diamict sediments were described and classified according to the scheme of Krüger & Kjær (1999). Clast fabrics were measured for elongated clasts with an *a/b* ratio of at least 1.5 and with an *a*-axis length ranging from 1 to 10 cm. Each clast fabric analysis consists of 25 observations and these were stereographically plotted on the lower hemisphere of a Lambert projection.

Age estimates were obtained by the Optically Stimulated Luminescence (OSL) technique (Table 1). Samples from sorted sediments were collected using plastic tubes (5 cm diameter and 30 cm long) and later analyzed at the Nordic Laboratory for Luminescence Dating, Risø, Denmark. After sample preparation and separation of quartz grains, measurements were made using the Single Aliquot Regenerated dose protocol (SAR) according to Murray *et al.* (1987) and Murray & Wintle (1999). It was assumed that the

samples had been completely saturated with water for 95% of the time after burial, which seems reasonable considering the present-day rapid coastal erosion. Furthermore, it is assumed, based on the grain size distribution, that after deposition, the water content in the sediment was 14-24% (Larsen *et al.* 1999).

Samples of the benthic foraminiferal species *Elphidium excavatum* from the four diamict elements were picked for amino acid analysis. The purpose was to improve the understanding of the absolute and relative ages, and in this way test the tectonic model. The samples were prepared according to the procedure described in Miller *et al.* (1983), and Sejrup & Haugen (1992), and subsequently run on an automatic amino acid analyzer. The degree of isoleucine epimerization is given as the ratio between D-alloisoleucine and L-isoleucine (aIle/Ile), measured as peak heights using a HP 3300 computing integrator. Only the total fraction was analyzed (Table 2).

Pollen samples (2.8 cm^3) had one *Lycopodium* tablet added for calculation of pollen concentration (Stockmarr 1971) and were treated with HF and acetolysed according to Fægri & Iversen (1989). Pollen identifications were based on those of Fægri & Iversen (1989) in combination with a reference collection of modern material. Phase contrast/oil immersion objectives (63x/1.4, 100x/1.3) and 10x oculars were used.

Description of architecture and sediments

Geometry of architectural elements

Four diamict beds or elements (DE_{1-4}) and three interbeds (I_{1-3}) of sorted sediments are identified between the Madakhá and Krinka rivers (Fig. 3). The distribution of diamict elements 1-3 is relatively uniform along the section, whereas the distribution of diamict element 4 is more limited. Where gullies intersect the coastal section, DE_{1-3} and I_{1-2} can be traced inland indicating that they have a tabular geometry. Both the lateral and vertical

variations of DE_{1-3} are mainly controlled by the architecture of I_1 and I_2, showing limited lateral persistence, and by the outline of I_3. Usually, the upper boundary of DE_1 is found above high tide level and rises to a maximum of 25 m a.s.l. Although the lower contact has not been observed, Diamict Element 1 is at least 10 m thick, and is bounded by the slightly undulating base of I_1 or DE_2. Diamict Element 2 is usually 10-15 m thick and its upper and lower boundaries are often conformable and parallel. Exceptions to the relatively uniform distribution occur due to undulations of the base of I_2, or where I_3 truncates DE_2. Diamict Element 3 is more variable with a thickness between 0-40 m, controlled by the variation of its base. Diamict Element 4 has a discontinuous lateral distribution and is only identified in the easternmost parts of the section where it is about 5 metres thick. The DE_4 can be traced further inland as exposed patches of diamict on the terrain surface. Interbed 1 exhibits a variable geometry, represented by deformed, sometimes folded lenses with a maximum thickness of 0.1-2 m and by a bed of relatively uniform thickness, about 10 m thick, which is subhorizontally truncated by DE_2. Interbed 2 is less variable than I_1 with a thickness up to 25 m. The geometry of I_3 is dominated by large-scale basin structures incised into the underlying sediment, sometimes as deep as 40 m. Between the main basins Interbed 3 is a thin bed about 1 metre thick and only covered where DE_4 is present (Fig. 3).

Basal contacts

Several major erosional surfaces can be traced along the section and are considered to be laterally continuous hiatuses. They form the basal contacts of individual diamict elements. The transition between the architectural elements DE_1 and DE_2 is characterised by shearing along both the lower and upper contacts of I_1 (Fig. 4). Where it reaches its maximum thickness, I_1 is undisturbed with the primary bedding intact. Deformation is restricted to narrow zones at its base and top (Fig. 5). Sometimes this is seen as a 1.5 m thick transitional

zone at the base of I_1, which consists of crudely banded diamict and sand with occasional folded sand lenses (Fig. 5B, C, D). Rotational features are recognized by clasts with wing-like appendages of diamict or sand indicating a sinistral sense of shear. Alternatively, I_1 is penetratively deformed resulting in numerous lenses of sand, boudinage structures, sheath folds or fold vergence all indicating progressive simple shear (van der Wateren *et al.* 2000). At these locations it is difficult to distinguish the bounding surfaces of the interbed as they are part of the transitional zone between DE_1 and DE_2. At other locations, I_1 is sharply overlain by a subhorizontal bed of slickensided mud up to one metre thick that, at its minimum thickness, separates DE_2 from the underlying sediments (DE_1) by only a few millimetres (Fig. 5A).

Similarly, the transition between DE_2 and DE_3 is characterised either by penetrative deformation of the entire I_2 or the deformation is restricted to zones at the bottom and top, leaving the internal part of I_2 intact with primary bedding preserved. Below the base of I_2, in DE_2, a zone with subvertical fracturing is overlain by a zone with subhorizontal fracturing. This is evident from their cross-cutting relationship. Fracture planes within the diamict are densely covered with slickensides. Where the transition is more strongly deformed it consists of a massive silty diamict and sand with silt laminae and lenses. It is characterised by extensional gravitational movement. Occasionally, the diamict component totally dominates its composition, while sand and mud only occur as thin lenses overprinted by normal faults. Otherwise the deformed sand and silt of I_2 is steeply inclined and folded with the diamict, and is also cut by a series of normal faults about 10 cm long. The upper contact of I_2 is a shear plane associated with shear lenses and tectonized mud with slickensided surfaces.

Interbed 3 truncates the underlying sediments as indicated by an angular unconformity related to the development of large-scale basins (Fig. 3). The transition is often marked by a gradation of diamict into mud with clasts affected by gravitational movements. Where I_3 is thin, primary bedded gravel and sand onlap the sharp contact to the underlying sediments.

Diamict element 4 has a well-defined, sharp, basal contact with a deformed zone affecting the upper metre of I_3 that shows overturned gravel, sand and mud (Fig. 5E).

Character of Diamict Elements

Diamict elements 1 to 4 are all massive, silty-clayey, firm, matrix-supported diamicts with moderate clast content and scattered fragments of shells. The colour is either bluish, grey or brownish with no distinction between individual diamict elements. Clasts larger than a few cm are rare except for occasional concentrations of densely striated larger clasts at basal and upper contacts. Most of the clasts are subangular and subrounded with frequent striations on their surfaces. Thin, deformed, one-metre-long sand lenses and bands of deformed dark grey mud occur, together with deformed stretched-out clasts about 10 cm-long. Thin lenses and horizons of sand are observed in DE_3 and DE_4, but only rarely. Nevertheless, rafts of dark grey deformed mud about 100 m long and 5-20 m thick occur within DE_3. Predominantly, the diamict has a compact appearance overprinted by both subvertical and subhorizontal fracture patterns. Sandstones and shales dominate the fine gravel content in all Diamict Elements. Calcareous rocks, mostly Palaeozoic limestone and black carbonates occur but are subordinate.

Character of Interbeds

Lacustrine and fluvial sediments**.** The lacustrine facies always overlies a diamict element, and fluvial sediments always overlie lacustrine sediments. Commonly, the lower part of the interbeds is composed of ripple and planar laminated silt and fine sand (Fig. 6). Climbing ripples indicate rapid sand accumulation (logs A and F in Fig. 6). In the middle part of the interbed, at site A, there is silt with interspersed dark brown sand layers. The colour is caused by a high content of organic matter including visible macro plant fragments. This organic

horizon has an erosive contact with the laminated beds below, as well as an erosive contact above with fine-grained sediments showing deformed ripples. At site B the lacustrine unit is cut erosively by several, 10-50 cm thick, fining upwards sets of trough cross-bedded gravel to sand. Measurements of sediment transport direction consistently point to a single source onshore relative to the present coastline.

The pollen diagram (Fig. 7) indicates considerable reworking: samples 02-519 (1-4), from the unit, contain predominantly secondary and poorly preserved microfossils such as bisaccate pollen, trilete spores, and pre-Quaternary pollen. Dinoflagellate cysts suggest a marine influenced origin. This unit is succeeded by a lacustrine depositional phase (samples 02-525(1-2)) containing high concentrations of well-preserved pollen. These assemblages show a progressive succession. Arboreal pollen (e.g. *Betula, Pinus, Picea*) increases, and the pioneer *Artemisia* decreases, suggesting a closure of the local vegetation. An open birch forest to birch-forest tundra with willows and tall herbs, is indicated, whereas the *Picea* increase suggests northwards advancing spruce. Collectively, this signals a warming trend.

Sedimentary structures indicate that the lower ripple and planar laminated silt and fine sand were deposited as lake sediments. The trough cross-bedded gravels and sands that cut down erosively into lake sediments are interpreted as fluvial in origin, and possibly represent a single channel. The fluvial sediment is probably a remnant of progradation across the lake sediments as the lake filled up. The observations indicate an environment with several shallow lakes that were filled rather rapidly with sediment.

Beach and shallow marine sediments. These comprise both gravelly and fine-grained facies, and are found overlying either diamict or lacustrine sediments (Fig. 6). About 4 metres of gravelly facies overlies erosively fine-grained lacustrine sediments. It consists of 20-50 cm thick bedsets of coarse gravel to medium sand. The bedsets are separated by low-angle bedding planes, which in some places are draped by 1-2 cm thick layers of massive silt. The

main bedding dips offshore relative to the present coastline, whereas tangential foresets and ripples are oppositely directed, more or less perpendicular to the present coastline, indicating bi-directional paleocurrents. Shell fragments are abundant throughout. At site H (Fig. 6), the sand to gravel bedsets are found between fine sand to mud. The lower and upper fine-grained units are in contact with diamict elements below and above. The two fine-grained sequences are deformed, but primary laminations and ripples, some with double mud drapes, are identifiable. The same type of fine-grained sediment is found as a 5.8 metres thick, internally undisturbed interbed at site C (Fig. 6). The unit is composed of heterolithic, very fine to medium-grained sand with mud drapes on ripple foresets. Double mud drapes and oppositely directed ripple foresets are common. Slightly larger asymmetrical wave ripples occur in the coarser sand about 1 metre above the base of the interbed.

The low-angle sand to gravel bedset unit is interpreted as beach sediment, the main bedding of which dips offshore from the present coast. The cross-bedding shows dunes migrating onshore. Below the beach sediments at site A (Fig. 6) there is 60 cm of alternating fine sand with weakly developed ripple structures, and massive sandy silt. The bedding is sub-horizontal with a bed thickness of 10-20 cm. This unit cuts down into organic lake sediments. The transition is interpreted as due to coastal erosion, turning a lacustrine basin into a marine embayment. The fine-grained, heterolithic sediment is interpreted as sub-tidal. Current ripples with double mud drapes on foresets are dominant reflecting slack water phases during flood and ebb current reversals (Nio & Yang 1991). The slightly asymmetrical, larger ripples in the unit are interpreted as wave ripples, indicating deposition above the fair weather wave base. The thin beach unit (site H in Fig. 6), which is composed of thin bedsets situated in between subtidal sediments, indicates that the facies variations were caused by lateral migration of the shallow water environments rather than sea-level change.

Reconstruction of paleoenvironments

Directional data and evidence of structural repetition

Ice flow directions are derived from intra-diamict clast fabric analyses, orientation of striation on clasts, slickensides, and the direction of minor folds and thrust planes. Indication of external ice pressure is determinable from both small and large-scale structures cross-cutting diamict elements and interbeds, or at the basal contacts of architectural elements. In the directional data set, two populations of orientation can be identified; one from the NW and another from the NE. The fabric analyses show that both directions have equal abundance in all diamict elements where neither lateral, nor vertical trends are recognised. However, a composite plot shows a dominance of the north-westerly direction (Fig. 8). Along the basal contacts, however, the directional sense of shear differs between individual architectural elements. Slickensides together with major thrust planes at the base of I_1 and DE_2 and thrust planes within DE_1 indicate a deformation from NW to SE. In contrast, the same features at the base of I_2 and DE_3 reflect NE to SW deformation directions (Figs 3, 8).

Mostly based on fabric orientations, we suggest that Diamict Element 1 was deposited from the NW and later overprinted by deformation involving shear along major thrust planes and sediment deformation from the NE. Thus it is possible that some of the clasts were re-oriented during thrusting from the NE. When the consistently oriented sense of shear along these contacts is considered, the simplest interpretation of the multiple till- and interbed alternation would be that it is due to a glaciotectonically induced repetition of the same till unit and its underlying deposits. Considering the subhorizontal basal contacts and the associated, relatively uniform distribution of diamict elements, development of a thrust complex must have involved the formation of large nappes, and transport of the substratum along thrust planes with a low inclination. This finds support in the striking similarities in facies composition between the individual diamict elements and interbeds in the investigated

section. The morphological properties and petrographic composition of the clasts are consistent in all diamict elements.

The following model is proposed for the architecture of the Kanin coastal sediments (Fig. 9):

A. Pre-deformation deposition of mud, lacustrine, fluvial and shallow marine sediments.

B. An ice sheet centred in the Barents Sea invaded mainland Russia from the NW and deposited a till in association with a deforming bed, i.e. deformation till. In the marginal zones of the ice sheet compressive flow was the dominant type of deformation. As the ice advanced, the marginal compressive structures were successively overridden and attenuated. We suggest that the variation in ice/bed coupling is reflected in the degree of extensional deformation seen within I_1 and I_2 extending as it does from internally undisturbed interbeds to boudinage, sheath and fold vergence structures (Boulton and Hindmarsh 1987; Hooke *et al*. 1997; Fischer *et al*. 2001).

C. When the ice sheet was advancing on to the Kanin area it moved up the adverse slope of the shelf, towards the Kanin ridge. This enhanced compression in the ice, and was reflected in compression within the sediments (Bluemle & Clayton 1984). When the applied shear stress exceeded the strength of the foreland sediments, dislocation of a large floe of the overlying sediments was initiated. The advancing glacier pushed a sub-horisontal nappe forward at a low angle on to the foreland. As tectonized mud is observed at the base of nappe structures, we speculate that weak mud acted as a medium for the décollement. Movement was probably facilitated by water-saturated mud at the décollement horizon, acting as a lubricator. It seems reasonable to assume that permafrost played an important role in the formation of the thrust complex as stiff foreland sediments were necessary to transmit glacial stress, and develop a width to depth ratio for the undeformed foreland wedge larger than 1:200 (Boulton *et al*. 1999; Bennett 2001). Irrespective of the presence of permafrost, the ice

sheet and its substratum acted as one single tectonic unit deformed by compression in a similar way to strata with a different competence (Bennett 2001). Most movement occurred along a major thrust plane located at the base of the nappe, but which was diverged from the sole thrust at the décollement surface. However, considerable displacement also took place within the nappe, along the weakness zone represented by the lithological boundary between till and sorted sediments. The overthrust sediments were subjected to compression resulting in small-scale reverse faulting, as seen in DE_1.

D. Another nappe was initiated and most of the deformation concentrated in narrow shear zones along major thrust planes resulting in structures showing a NW sense of shear. The distal part of the nappes that were exposed to the foreland of the glacier and may have been subject to normal faulting and slumping, and this would have overprinted the signature of the subhorizontal thrust planes (c.f. van der Wateren 1985). The adverse slope of the foreland allowed proglacial meltwater to run parallel to the ice front, further encouraging slumping. It is likely that slumping occurred contemporary to thrusting, considering the sharp base of DE_3, cutting the slumped I_2. However, glacially induced stress must have reactivated part of this upper nappe as NW trending structures along the thrust plane were overprinted by a NE sense of shear as seen in the lower parts of I_2 and the upper parts of DE_1.

E. After deglaciation, large drainage systems from the inland cut down into the thrust complex, and basins were filled with stratified, lacustrine sediments. Flows of saturated sediments along the basin slopes occurred both prior to and simultaneous with the infilling. This can be concluded from the transitional nature of the base of I_3. A final ice advance from the NW or NE moved on to the mainland and deposited DE_4 on top of the infilled basins, incising the thrust complex.

F. When the ice had left the southern Barents Sea, the northward drainage pattern of the Kanin ridge was re-established. Minor rivers incised the Quaternary succession forming narrow gullies, while major rivers formed large fluvial terraces.

Depositional model and age of fine-grained sediments

Given that the glacial tectonic model (Fig. 9) is valid, interbeds 1 and 2 derive from the same stratigraphic succession. We suggest deposition in a setting quite similar to the present day along the north coast of the Kanin Peninsula for the sequences observed within the two interbeds (Fig. 10). This depositional model infers rapid coastal retreat and marine capturing of lakes forming small marine embayments.

Lacustrine sedimentation took place in shallow lakes close to the coastline (Fig. 10). The lakes rapidly filled in by lacustrine and fluvial sediments. Lakes that were not completely filled with sediment were turned into small marine embayments with shallow water marine sedimentation as the coastline retreated. Large sediment input by rivers in combination with tidal currents resulted in the deposition of tidally dominated sediments. Sub-tidal rippled sediments are common. Sandy foreshore sediments sandwiched between more fine-grained sub-tidal sediments are interpreted as due to lateral migration of the shallow marine facies. In fact, all observations concerning the interbeds can be interpreted in terms of lateral variations in the sedimentation patterns of a number of small lakes and marine embayments on either side of a retreating coastline. As the sediments are found in dislocated interbeds, basin and coastline configurations cannot be established accurately from paleocurrent measurements. However, paleocurrent measurements are directed offshore relative to the present coastline, or both on- and offshore in cases of oppositely directed currents. The present coastline (and profile) is oriented east – west, almost parallel to the strike of the thrust nappes. Thus, it can

be concluded that the coastline, during deposition of the successions found as interbeds, was located north of the present one, but ran more or less parallel to it.

OSL dates from interbeds 1 and 2 range in age from 92 to 188 ka (Fig. 6, Table 1), but do not allow any firm conclusion to be drawn, although the data set would support the interpretation that the sediments are approximately Eemian in age. Amino acid ratios from shells and foraminifera are widely used to obtain chronological information (e.g. Sejrup *et al.* 1987; Larsen *et al.* 2000). The amino acid ratios on samples of *Elphidium excavatum* from the diamict elements fall into two distinct groups around 0.035 and 0.090 (Table 2). The fossils in diamict elements 1-3 may derive from marine sediments belonging to interbeds 1 and 2 and/or from an older marine unit. The marine fossils in Diamict Element 4 may be younger or be re-sedimented from the same marine unit. The two amino acid clusters do not distuingish between interbeds 1-2 and interbed 3 (Table 2). Interestingly, all high values are at 11 m a.s.l. and lower, whereas the low values are found at 29 m a.s.l. and higher. This introduces the possibility that both groups derive from the same ice-free period, and that the high values relate to higher temperatures due to a transgression in the Middle Weichselian (Kjær *et al.* 2003; Jensen *et al.* this issue). However, it cannot be excluded that the two groups represent two different ice-free periods. There are no amino acid results from stratigraphically well-constrained sites on the Kanin Peninsula for comparison, only one analysis on *Arctica islandica* is reported (Miller & Mangerud 1985). The values from the Pyoza river area (Fig. 1) on *Elphidium excavatum* in Eemian sediments are somewhat higher than the low values in Table 2 (H.P. Sejrup, pers. comm. 2004).

The dislocated terrestrial and shallow marine sediments were deposited below the level where they are now found (0-60 m a.s.l.), i.e. below the present sea level. According to the glacial geological model, the sediments were dislocated by the first Weichselian ice advance in the area. Thus, the simplest interpretation is that the sediments were deposited

some time in the Late Saalian (deglacial) – Eemian – Early Weichselian (pre-glacial) interval. A relative sea level much higher than present day one has been demonstrated for the Saalian – Eemian (Funder *et al.* 2002; Grøsfjeld *et al.* this issue; Larsen *et al.* this issue). During the Late Eemian – Early Weichselian the sea level fell below the present level. The coastal retreat inferred from the sedimentation pattern (Fig. 10) is at odds with a falling sea level, meaning that a standstill or transgression must have taken place during an overall regressive phase. The vegetational development (Fig. 7) cannot be used to discriminate further because the information in the diagram presented is too sparse, and partly because little is known about vegetational development at these latitudes in the period Late Saalian to Early Weichselian (Nikonov & Vostrukhina 1964 (in Ikonen & Ekman 2001); Yevzerov *et al.* 1976 (in Ikonen & Ekman 2001)).

Conclusions

Glaciotectonic thrusting at a scale only known from marine seismic investigations was traced in an approximately 20 km long section. This thrusting by the Barents Sea and Kara Sea Ice sheets took place in Early to Middle Weichselian time. Due to the resulting dislocation, stratigraphically older sorted sediments occur in two discrete interbeds between diamict elements. These sediments are of lacustrine, fluvial and shallow marine origin, probably of Early Weichselian age. The record from the interbeds indicates a sedimentation that started in lake basins, and continued in shallow marine embayments as the lakes opened to the sea. Sedimentation occurred at an elevation below the present sea level. The coastline at the time was located to the north of the present day one, and ran sub-parallel to it. The transition from lacustrine to shallow marine sedimentation might represent a marine transgression, but the style of sedimentation recorded might also be explained in terms of a stable sea level and coastal erosion causing marine capturing of lake basins. The pollen record, although sparse

and indicative of a slight warming trend, would represent interstadial rather than full interglacial conditions.

Acknowledgements. – This project is a contribution to the "QUEEN" project (Quaternary Environment of the Eurasian North) – a network project within the European Science Foundation. The project was funded through the European Community project "Eurasian Ice Sheets" (contract ENV4-CT970563), the Norwegian Research Council, the Danish Natural Science Research Council through the "CLIENT " and "TripleJunction" projects, the Swedish Polar Secretariat, The Norwegian Barents Secretariat, and the Swedish Crafoord Foundation. Numerous discussions with colleagues from the QUEEN project contributed significantly to the work. Luminescence dating was carried out at the Nordic Laboratory for Luminescence Dating, Risø, Denmark. Amino acid analyses were performed at the Amino Acid laboratory at the University of Bergen. Anne Nordtømme, Geological Survey of Norway, prepared pollen samples. Erik Hårberg, Geological Survey of Norway, helped with figures 1 and 10. Comments by the journal referees, Drs. John F. Hiemstra and Jon Landvik, were a great help in improving the manuscript. Peter Padget corrected the English.

References

Astakhov, V. 2001: The stratigraphic framework for the Upper Pleistocene of the glaciated Russian Arctic: changing paradigms. *Global and Planetary Change 31,* 283-295.

Bennett, M.R. 2001: The morphology, structural evolution and significance of push moraines. *Earth-Science Reviews 53,* 197-236.

Bluemle, J.P. & Clayton, L. 1984: Large-scale glacial thrusting and related processes in North Dakota. *Boreas 13,* 279-299.

Boulton, G.S. & Hindmarsh 1987: Sediment deformation beneath glaciers: Rheology and geological consequences. *Journal of Geophysical Research 92B,* 9059-9082.

Boulton, G.S., van der Meer, J.J.M., Beets, D.J., Hart, J.K. & Ruegg, G.H.J. 1999: The sedimentary and structural evolution of a recent push moraine complex: Holmströmsbreen, Spitsbergen. *Quaternary Science Reviews 18,* 339-371.

Boyce, J.I. & Eyles, N. 2000: Architectural element analyses applied to glacial deposits: Internal geometry of a late Pleistocene till sheet, Ontario, Canada. *Geological Society of America Bulletin 112,* 98-118.

Eyles, N., Eyles, C.H. & Miall, A.D. 1983: Lithofacies types and vertical profile models; an alternative approach to the description and environmental interpretation of glacial diamict and diamictite sequences. *Sedimentology 30,* 395-410.

Fischer, U.H., Porter, P.R., Sculer, T., Evans, A.J. & Gudmundsson, G.H. 2001: Hydraulic and mechanical properties of glacial sediments beneath Unteraargletcher, Switzerland: Implications for glacier basal motion. *Hydrological Processes 15,* 3225-3540.

Funder, S., Demidov, I. & Yelovicheva, Y. 2002: Eemian mollusc faunas and hydrography of the Baltic and the White Sea – North Sea seaway. *Palaeogeography, Palaeoclimatology, Palaeoecology 184,* 275-304.

Fægri, K. & Iversen, J. 1989: *Textbook of pollen analysis*. 4. revised edition by Fægri, K., Kaland, P.E., & Krzywinski, K. Wiley, Chichester. 314 pp.

Gataullin, V., Mangerud, J. & Svendsen, J.I., 2001: The extent of the Late Weichselian ice sheet in the southeastern Barents Sea. *Global and Planetary Change 31*, 453-474.

Grøsfjeld, K., Funder, S., Glaister, C., Nielsen, J.K. & Seidenkranz, M.S.: Last interglacial marine environments in the White Sea region, northern Russia. *Boreas,* this volume.

Hooke, R.L., Hanson, B., Iverson, N.R., Janson, P. & Fischer, U.H. 1997: Rheology of till beneath Storglaciären, Sweden. *Journal of Glaciology 43*, 172-179.

Ikonen, L. & Ekman, I. 2001: Biostratigraphy of the Mikulino interglacial sediments in NW Russia: The Petrozavodsk site and a literature review. *Annales Academiae Scientiarum Fennicae Geologica-Geographica 161*. Helsinki. 88 pp.

Jensen *et al.* this volume

Kamb, W.B. 1959: Ice petrofabric observations from Blue Glacier, Washington, in relation to theory and experiment. *Journal of Geophysical Research, 64,* 1891-1909.

Kjær, K.H., Demidov, I.N., Larsen, E., Murray, A. & Nielsen, J.K. 2003: Mezen Bay – a key area for understanding Weichselian glaciations in northern Russia. *Journal of Quaternary Science 18,* 73-93.

Kjær *et al.* this volume

Krüger, J. & Kjær, K.H. 1999: A data chart for field description and genetic interpretation of glacial diamicts and associated sediments – with examples from Greenland, Iceland, and Denmark. *Boreas 28,*386-402.

Larsen et al. this volume.

Larsen, E., Lysså, A., Demidov, I., Funder, S., Houmark-Nielsen, M., Kjær, K.H. & Murray, A.S. 1999: Age and extent of the Scandinavian ice sheet in northwest Russia. *Boreas 28,* 115-132.

Larsen, E., Sejrup, H.P., Janocko, J., Landvik, J.Y., Stalsberg, K. & Steinsund, P.I. 2000: Recurrent interaction between the Norwegian Channel Ice Stream and terrestrial-based ice across southwest Norway. *Boreas 29,* 185-203.

Lavrushin, Yu.A. & Epstein, O.G. 2001: Pleistocene geological events of northeastern Europe and southern Barents Sea (recorded in naturally occurring key sections). *Bulletin of the Commission for Quaternary studies of the Russian Academy of Science 64,* 35-50.

Miall, A.D. 1988: Architectural elements and bounding surfaces in fluvial deposits: Anatomy of the Kayenta formation (Lower Jurassic), southwest Colorado. *Sedimentary Geology 55,* 233-262.

Miller; G.H. & Mangerud, J. 1985: Aminostratigraphy of European marine interglacial deposits. *Quaternary Science Reviews 4,* 215-278.

Miller, G.H., Sejrup, H.P., Mangerud, J. & Andersen, B.G. 1983: Amino acid ratios in Quaternary molluscs and foraminifera from western Norway: correlation, geochronology and paleotemperature estimates. *Boreas 12,* 107-124.

Murray, A.S, Marten, R., Johnston, A. & Martin, P. 1987: Analysis for naturally occurring radionuclides at environmental concentrations by gamma spectrometry. *Journal of Radioanalytical and Nuclear Chemistry, Articles 115,* 263-288.

Murray, A.S. & Wintle, A.G. 1999: Luminescence dating of quartz using an improved singlealiquot regenerative-dose protocol. *Radiation Measurements 32,* 57-73.

Nio, S.-D. & Yang, C.-S. 1991. Diagnostic attributes of clastic tidal deposits: a review. *In* Smith, D.G., Reinson, G.E., Zaitlin, B.A. & Rahmani, R.A. (eds.): Clastic tidal sedimentology. *Canadian Society of Petroleum Geologists, Memoir 16,* 3-28.

Ramsey, W. 1904: Beiträge zur Geologie der recenten und pleistocänen Bildungen der Halbinsel Kanin. *Bulletin de Société de Géographie de Finlande, Fennia 21,* 1-66.

Sejrup, H. P., I. Aarseth, I., Ellingsen, K.L., Reither, E. & Jansen, E. 1987: Quaternary stratigraphy of the Fladen area, central North Sea: A multidisciplinary study. *Journal of Quaternary Science 2,* 35-58.

Sejrup, H. P. & Haugen, J.-E. 1992: Foraminiferal amino acid stratigraphy of the Nordic Seas: Geological data and pyrolysis experiments. *Deep Sea Research 39,* 603-623.

Spiridonov, M.A. & Yakovleva, S.V. 1961: Quaternary deposits of the Kanin Peninsula shore and Peza River Basin. *In* Yakovleva S.V. (ed.): Materials on Quaternary Geology and Geomorphology of the USSR. *VSEGEI Leningrad, 75-89.* (Translated).

Stockmarr, J. 1971: Tablets with spores in absolute pollen analysis. *Pollen et Spores 13,* 615-621.

Svendsen, J.I., Alexanderson, H., Astakhov, V.I., Demidov, I., Dowdeswell, J.A., Funder, S., Gataullin, V., Henriksen, M., Hjort, C., Houmark-Nielsen, M., Hubberten, H.W., Ingólfsson, Ó., Jakobsson, M., Kjær, K.H., Larsen, E., Lokrantz, H., Lunkka, J.P., Lysså, A., Mangerud, J., Matioushkov, A., Murray, A., Möller, P., Niessen, F., Nikolskaya, O., Polyak, L., Saarnisto, M., Siegert, C., Siegert, M.J., Spielhagen, R.F. & Stein, R. 2004: Late Quaternary ice sheet history of northern Eurasia. *Quaternary Science Reviews 23,* 1229-1271.

Sættem, J. 1990: Glaciotectonic forms and structures on the Norwegian continental shelf: observations, processes and implications. *Norsk Geologisk Tidsskrift 70*, 81-94.

Van der Wateren; F.M., Kluvinng, S.J. & Bartek, L.R. 2000: Kinematic indicators of subglacial shearing. *In* Maltmann A.J., Hubbard, B. & Hambrey, M.J. (eds.): Deformation of glacial materials. *Geological Society of London, Special Publications 176*, 256-278.

Figure captions

1. Part of northwest Russia showing the location of the investigated, 18.7 km long section between the outlets of the rivers Madakhá and Krinka on the north coast of the Kanin Peninsula.
2. A. Oblique photo showing part of the investigated section. B. The section showing the succession at 5400 metres (cf. Figs 3, 6).
3. Geological sections of the northern coast of Kanin between Madakhá (zero metres) and Krinka (18700 metres) rivers showing outcrop of the different architectural elements: Diamict Element (DE) 1-4 and Interbeds (I) 1-3. Logs A-H refer to detailed sedimentological logging of interbed 1 and 2. See Figs 6, 7.
4. Diagrams showing the variation of basal contacts between diamict elements and interbeds; $DE_1 – DE_2$ and $DE_2 – DE_3$.
5. Basal contacts. A. The contact between DE_1 and DE_2 only separated by a mud layer a few millimetres thick and overprinted by slickensides. The ruler is 2 metres long. B. Basal contact of interbed 1 at 5400 metres. Above the sharp contact to a sandy facies of the interbed, the primary bedding is intact. At and below the boundary, sand lenses are folded towards the east, and this is related to the rotation of many structures which indicate movement along the base of interbed 1. C. Detail from the contact showing rotated clast with attached appendages of diamict. D. Rotated clast indicating sinistral shear along sharp contact between diamict and sand. E. Glacial tectonic unconfomity between diamict element 4 and interbed 3 with erosion and overturned folds in gravel and sand.
6. Sedimentary logs from interbed 1 (A – C) and interbed 2 (D – H). Numbers below each letter represent distance in metres measured along the section from the outlet of

the river Madakhá. The positions of logs are also marked on the profile sketches (Fig. 3). Vertical scales in logs are metres above high tide. Photos show lacustrine sediments with organic material and beach sediments (log A), and tidal sediments with typical double mud drapes on ripple fore-sets (log C).

7. Pollen percentage diagram of selected taxa, total pollen concentration, spores and secondary microfossils from lacustrine sediments in interbed 1 at site A (Fig. 6). Shaded curves are 10x exaggeration of the scale.
8. Compilation of directional data measured along the section between Madakhá and Krinka including: folds and thrust planes of internal and external structures, slickensides along boundaries, striation on clasts within diamict elements and composite diagrams with clast fabrics from DE_1 (N=9); DE_2 (N=8); DE_3 (N=11). Composite fabric diagrams were constructed by plotting all fabric data from each Diamict Element into one diagram. Except for two clast fabrics in DE_3 all fabric analyses show significant preferred orientation with no systematic lateral or vertical variation along the section. Contoured diagrams after Kamb (1959) using three and six times the standard deviation for random distribution.
9. Glaciotectonic model for the architecture of the Kanin thrust complex. A-F shows the sequential development from Late Saalian to Middle Weichselian.
10. Depositional model explaining how the transition from lacustrine and fluvial sedimentation to marine sedimentation found within interbeds 1 and 2 is caused by coastal retreat.

Tables

1. Optically Stimulated Luminescence (OSL) dates obtained from interbeds 1 and 2. Sample numbers starting with 02 denote samples collected in the year 2002. These dates are plotted on the sedimentary logs (Fig. 6). Sample numbers starting with 00 denote samples collected in the year 2000 from the same two interbeds, but these are not plotted.

2. Amino acid ratios obtained from samples of *Elphidium excavatum* extracted from diamict elements 1-4 underlying, separating and overlying interbeds (cf. Fig. 3). Note that only the total hydrolysed fraction was analysed.

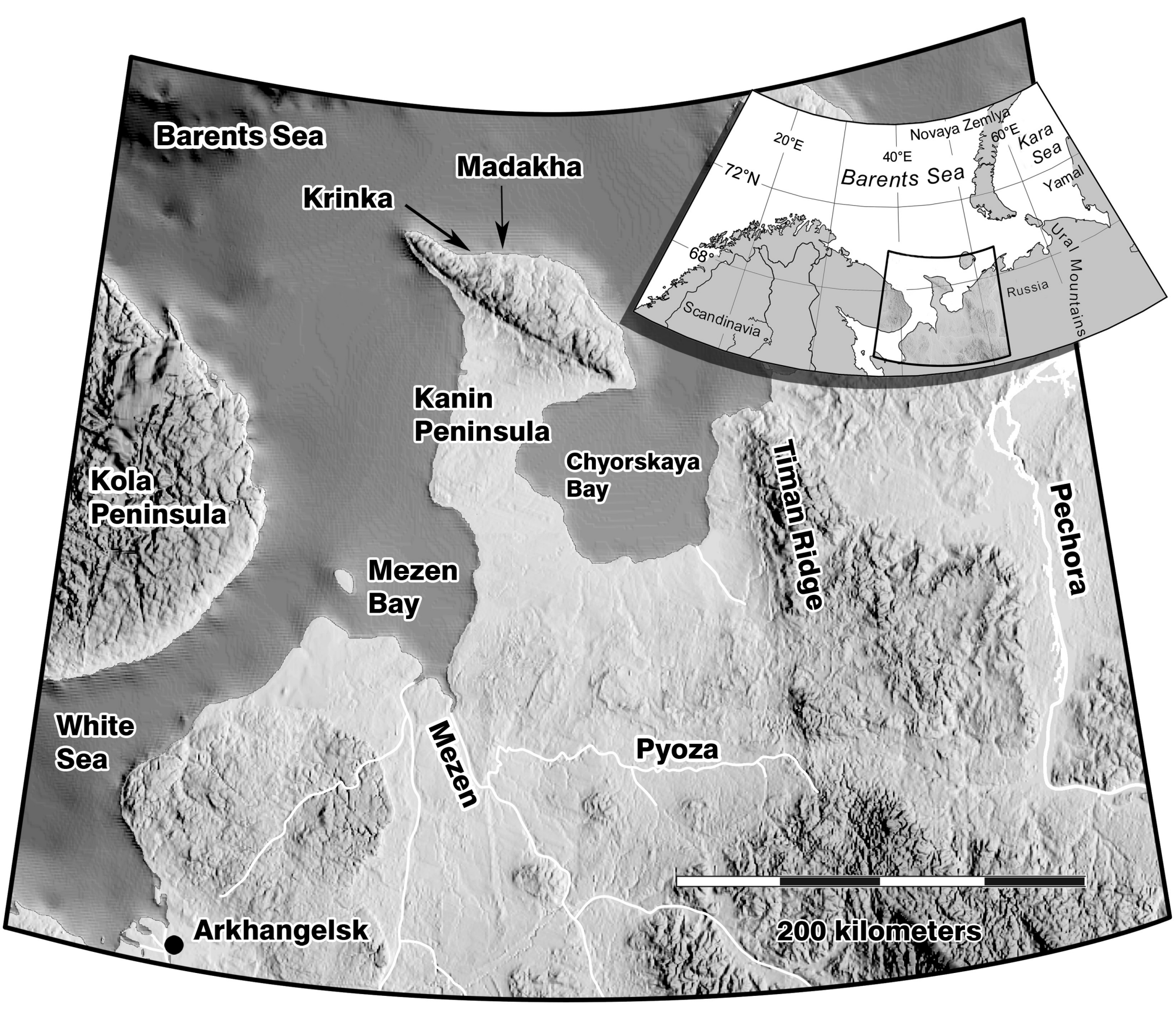
Barents Sea
Madakha
Krinka
Kanin Peninsula
Chyorskaya Bay
Kola Peninsula
Mezen Bay
Timan Ridge
Pechora
White Sea
Mezen
Pyoza
Arkhangelsk
200 kilometers
20°E
40°E
60°E
72°N
68°
Novaya Zemlya
Kara Sea
Barents Sea
Yamal
Ural Mountains
Russia
Scandinavia

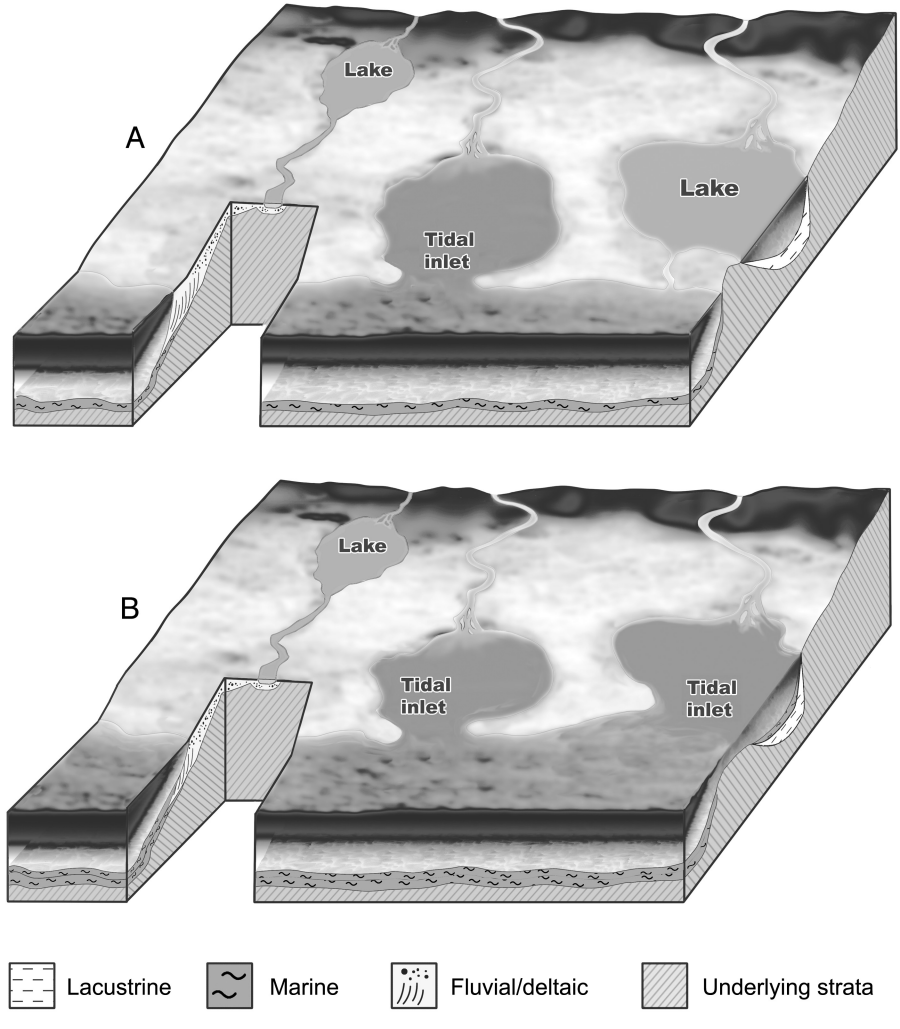
A
Lake
Lake
Tidal inlet
B
Lake
Tidal inlet
Tidal inlet
Lacustrine
Marine
Fluvial/deltaic
Underlying strata

A

B

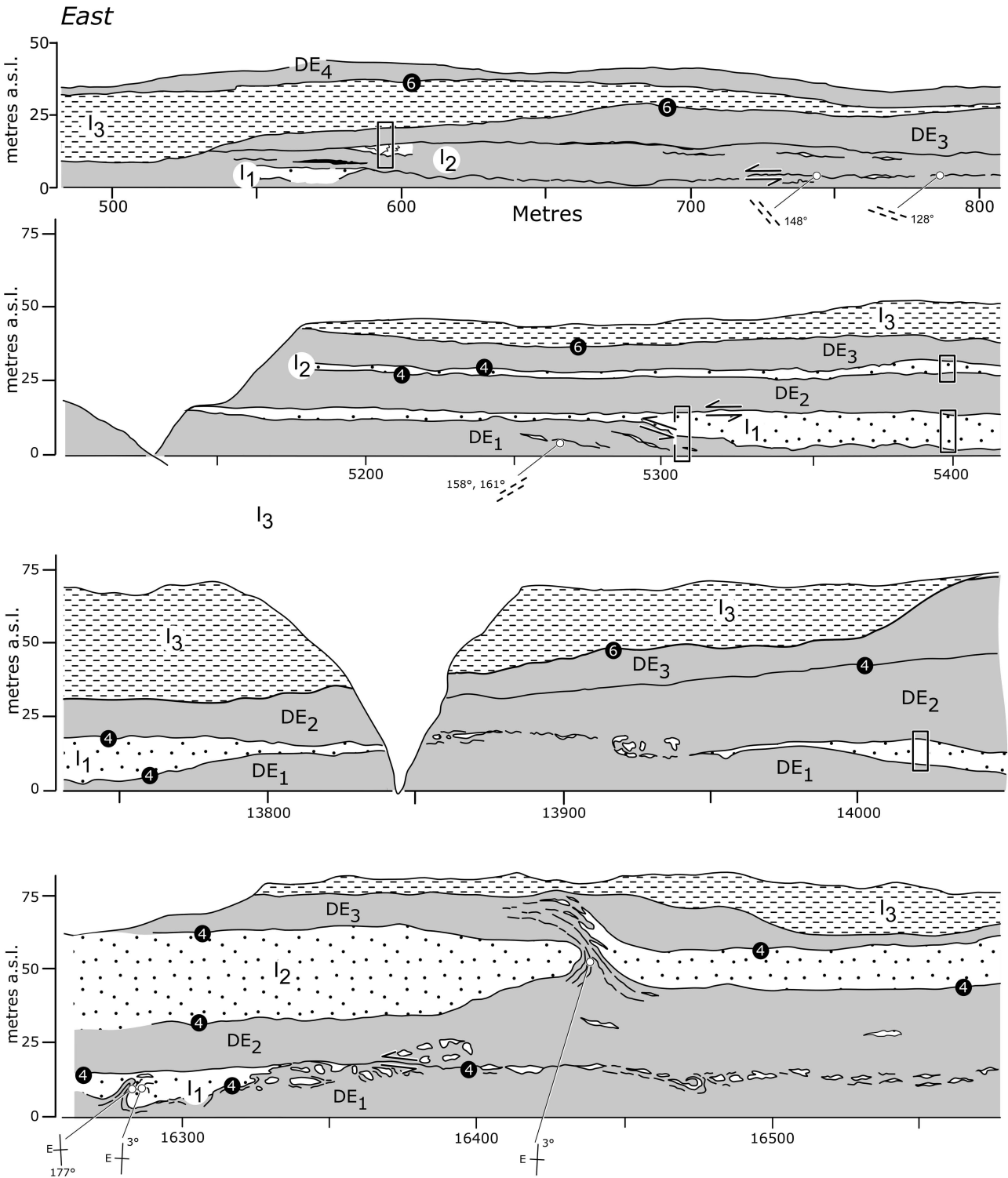
East
metres a.s.l.
50
25
0
DE4
DE3
I3
I2
I1
6
500
600
Metres
700
800
148°
128°
75
50
25
0
5200
5300
5400
158°, 161°
DE2
DE1
4
I3
13800
13900
14000
16300
16400
16500
E
177°
3°

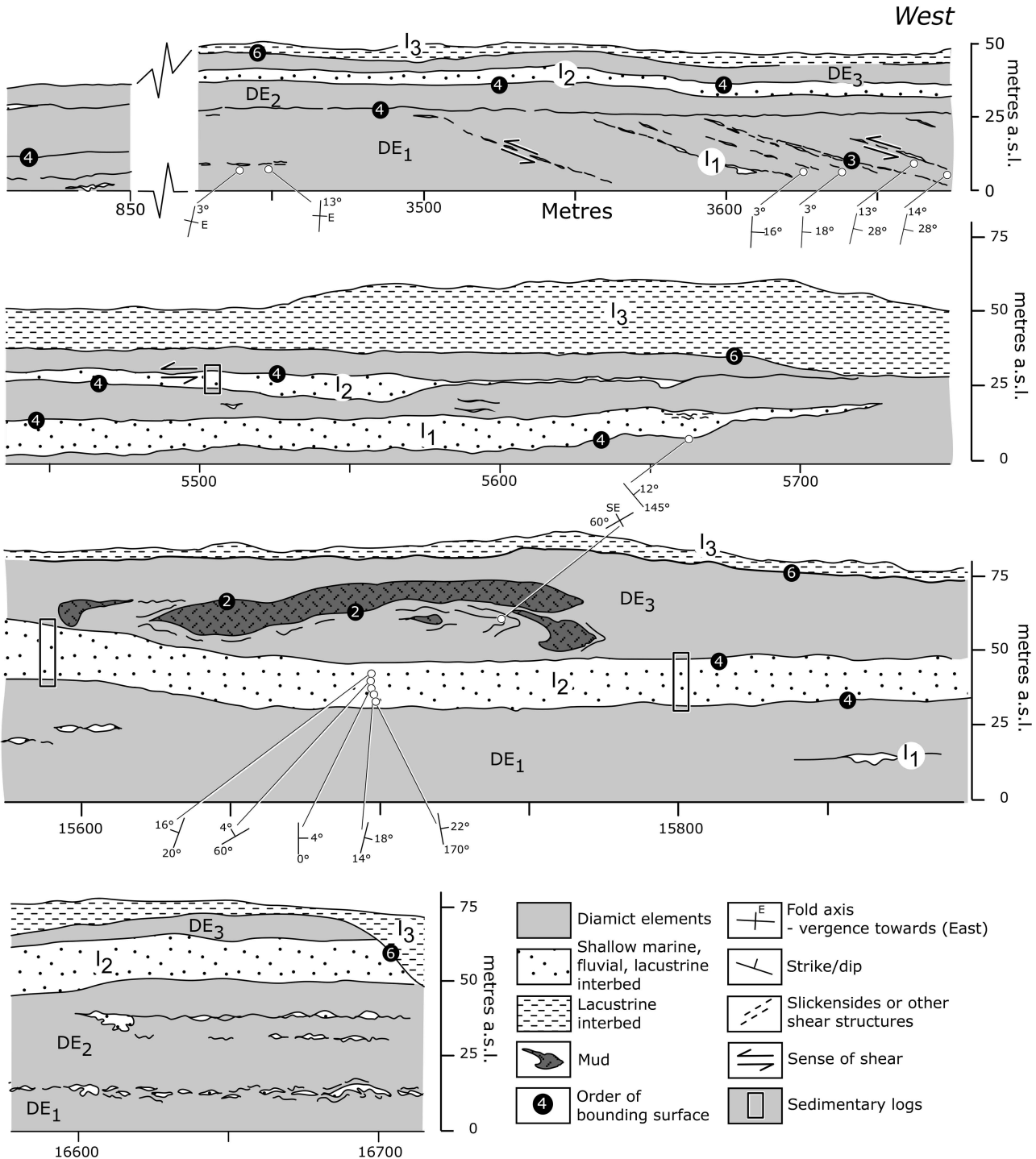
West
I3
I2
I1
DE3
DE2
DE1
6
4
3
2
50
25
0
metres a.s.l.
75
850
3500
Metres
3600
5500
5600
5700
15600
15800
16600
16700
3° E
13° E
3°
16°
18°
13°
28°
14°
28°
12°
145°
SE
60°
4°
20°
60°
0°
14°
18°
22°
170°
Diamict elements
Shallow marine, fluvial, lacustrine interbed
Lacustrine interbed
Mud
Order of bounding surface
Fold axis - vergence towards (East)
Strike/dip
Slickensides or other shear structures
Sense of shear
Sedimentary logs

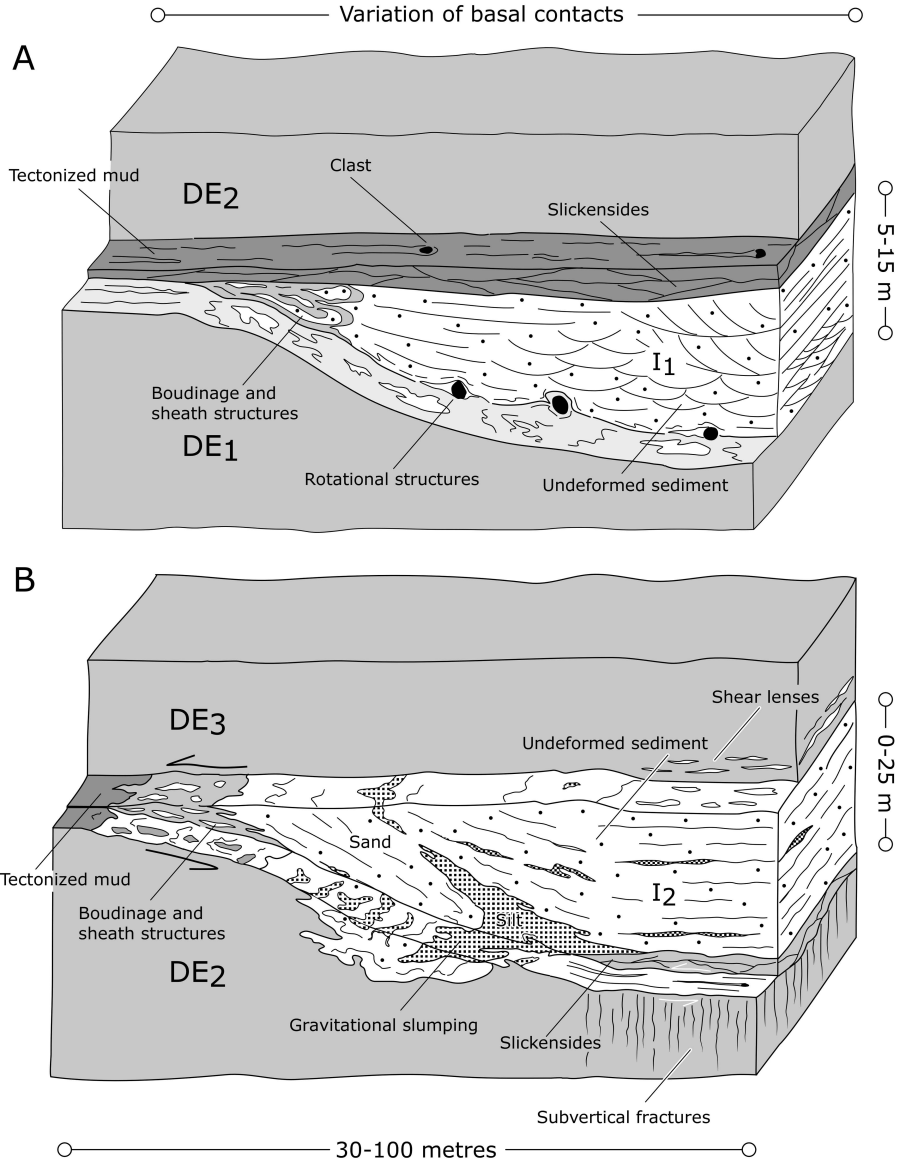
Variation of basal contacts
A
Tectonized mud
Clast
DE2
Slickensides
5-15 m
I1
Boudinage and
sheath structures
DE1
Rotational structures
Undeformed sediment
B
DE3
Shear lenses
Undeformed sediment
0-25 m
Sand
Tectonized mud
I2
Boudinage and
sheath structures
Silt
DE2
Gravitational slumping
Slickensides
Subvertical fractures
30-100 metres

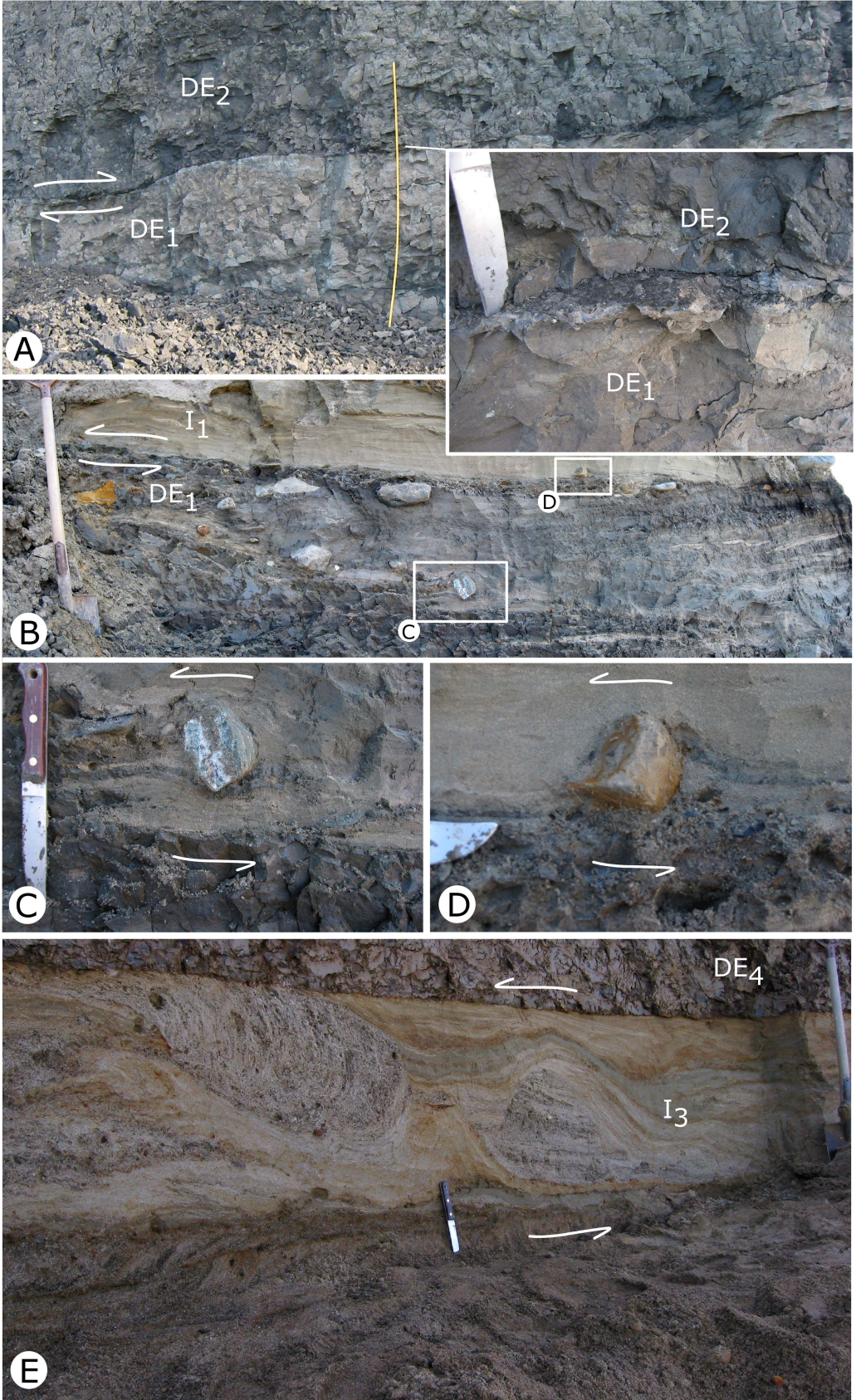
DE2
DE1
A
DE2
DE1
I1
DE1
D
B
C
C
D
DE4
I3
E

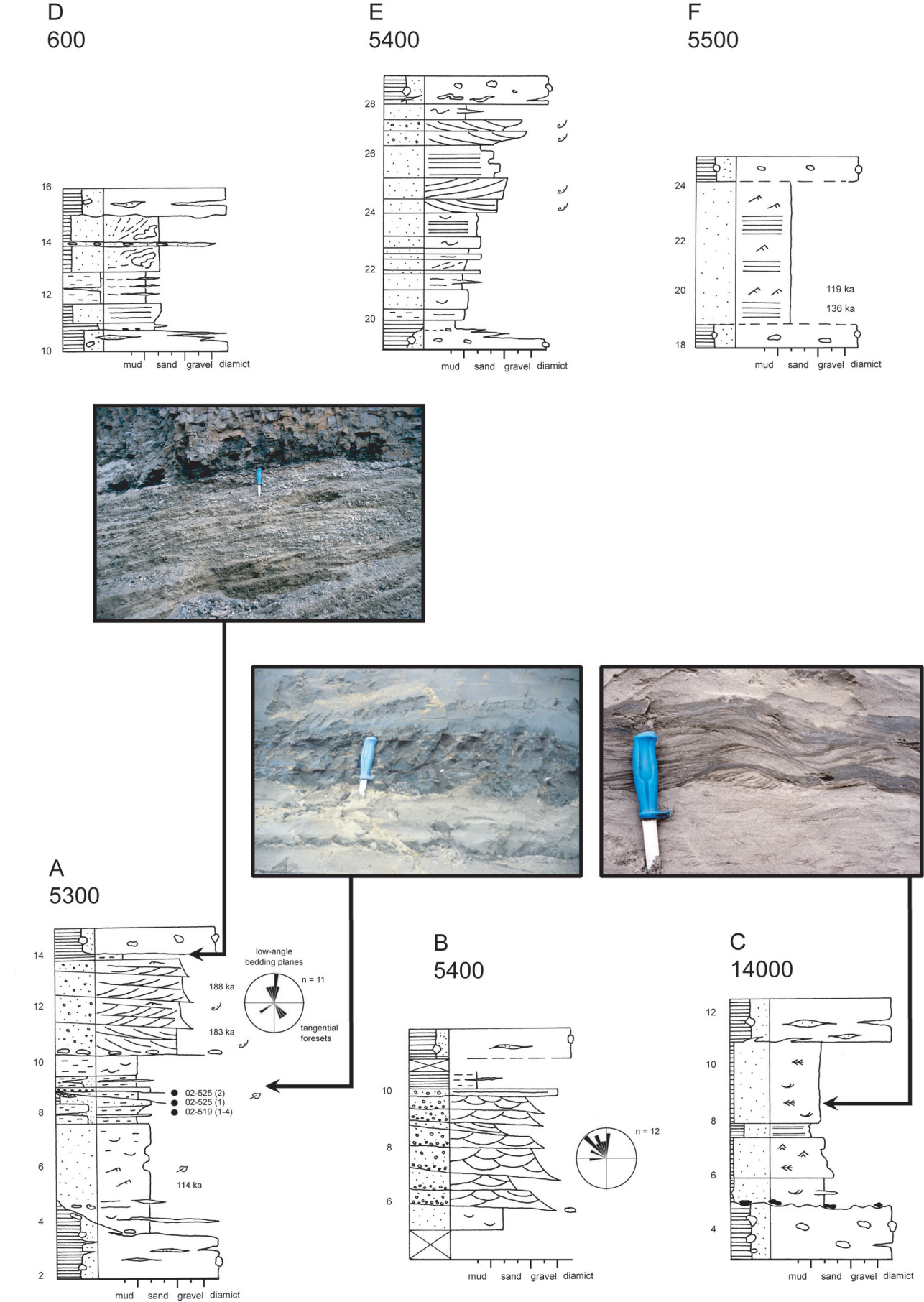
D
600
16
14
12
10
mud
sand
gravel
diamict
E
5400
28
26
24
22
20
mud
sand
gravel
diamict
F
5500
24
22
20
18
119 ka
136 ka
mud
sand
gravel
diamict
A
5300
14
12
10
8
6
4
2
188 ka
183 ka
114 ka
low-angle
bedding planes
n = 11
tangential
foresets
02-525 (2)
02-525 (1)
02-519 (1-4)
mud
sand
gravel
diamict
B
5400
10
8
6
n = 12
mud
sand
gravel
diamict
C
14000
12
10
8
6
4
mud
sand
gravel
diamict

G
15600

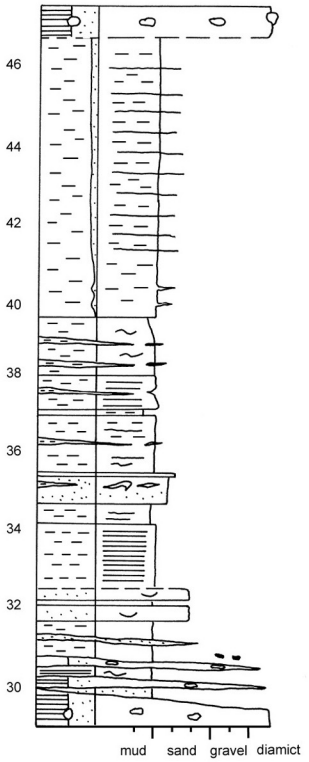

H
15800

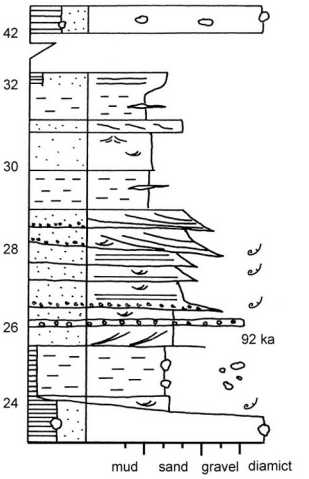

Legend

heterolithic beds
mud
silt
sand
gravel
diamict

boundary not exposed

unexposed

massive

horizontal bedding

weakly laminated

tangential cross-bedding

cross-bedding with double mud drapes

trough cross-bedding

ripples

ripples with double mud drapes

climbing ripples

wave ripples

herringbone cross-bedding

slump

peat lense

water escape structure

shell fragments

plant detritus

mud clasts

clast

N
sediment transport directions

pollen sample

92 ka
luminescence age

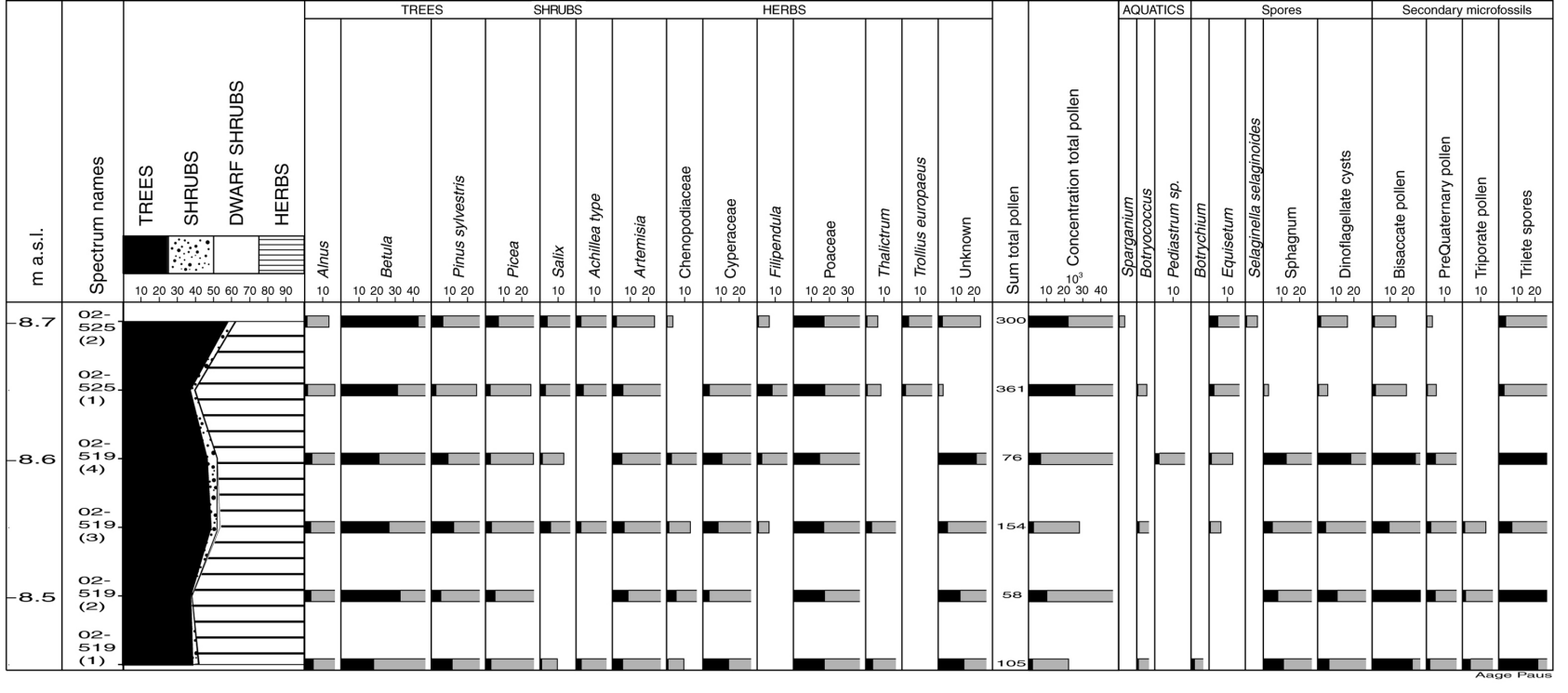
m a.s.l.
Spectrum names
TREES
SHRUBS
DWARF SHRUBS
HERBS
10 20 30 40 50 60 70 80 90
TREES
SHRUBS
HERBS
Alnus
Betula
Pinus sylvestris
Picea
Salix
Achillea type
Artemisia
Chenopodiaceae
Cyperaceae
Filipendula
Poaceae
Thalictrum
Trollius europaeus
Unknown
Sum total pollen
Concentration total pollen
10^3
AQUATICS
Sparganium
Botryococcus
Pediastrum sp.
Spores
Botrychium
Equisetum
Selaginella selaginoides
Sphagnum
Dinoflagellate cysts
Secondary microfossils
Bisaccate pollen
PreQuaternary pollen
Triporate pollen
Trilete spores
8.7
8.6
8.5
02-525 (2)
02-525 (1)
02-519 (4)
02-519 (3)
02-519 (2)
02-519 (1)
300
361
76
154
58
105
Aage Paus

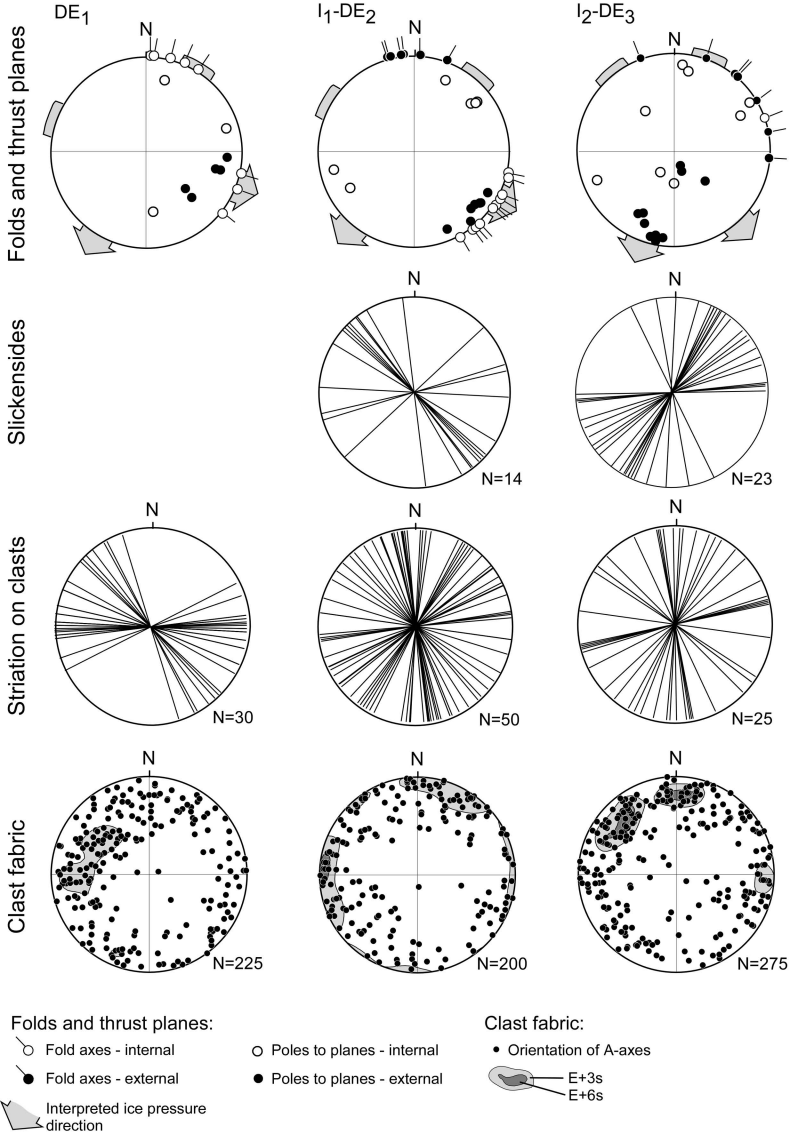
DE1
I1-DE2
I2-DE3
Folds and thrust planes
Slickensides
Striation on clasts
Clast fabric
N
N=14
N=23
N=30
N=50
N=25
N=225
N=200
N=275
Folds and thrust planes:
Fold axes - internal
Fold axes - external
Interpreted ice pressure direction
Poles to planes - internal
Poles to planes - external
Clast fabric:
Orientation of A-axes
E+3s
E+6s

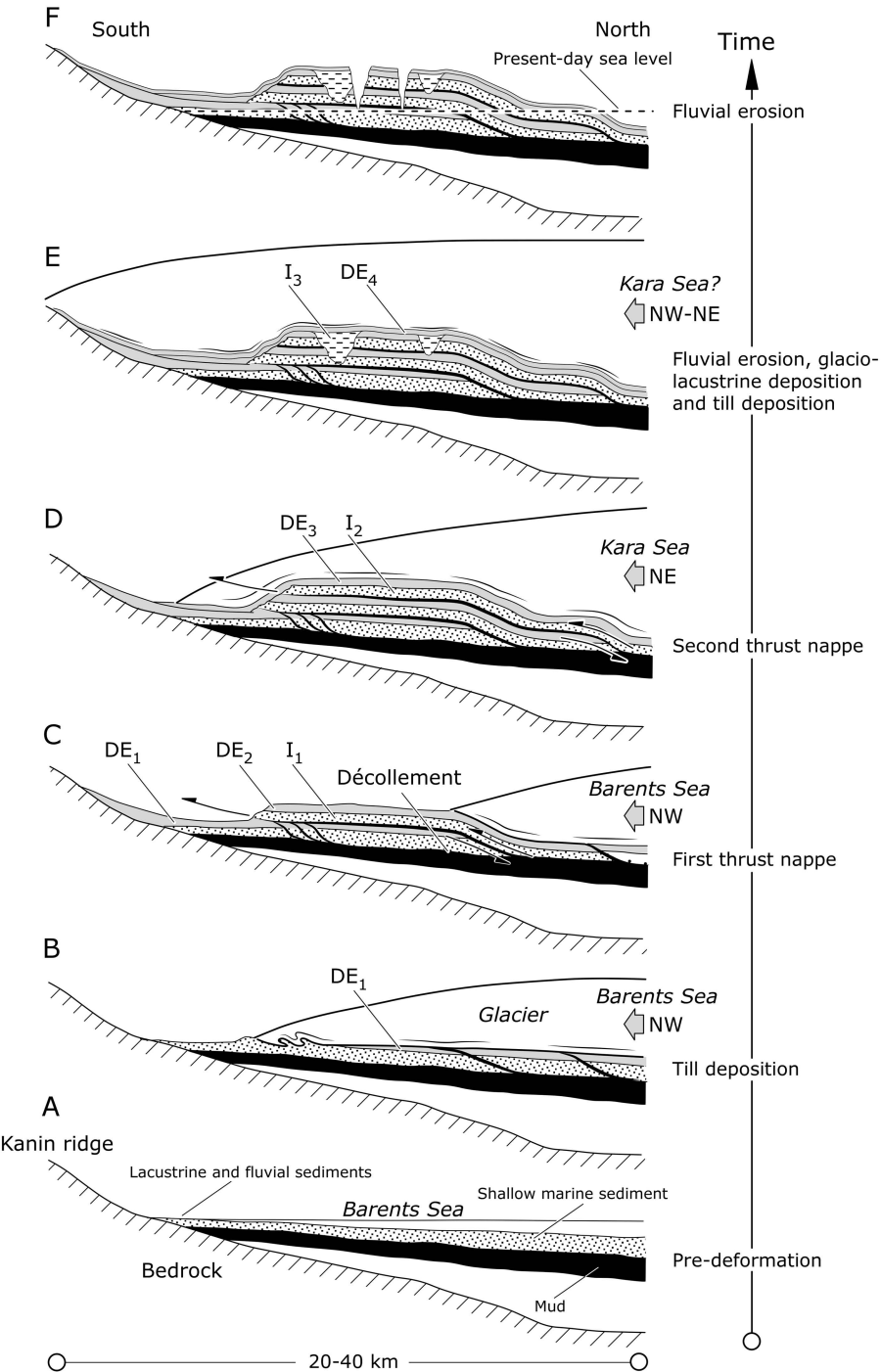
F
South
North
Present-day sea level
Time
Fluvial erosion
E
I3
DE4
Kara Sea?
NW-NE
Fluvial erosion, glacio-lacustrine deposition and till deposition
D
DE3
I2
Kara Sea
NE
Second thrust nappe
C
DE1
DE2
I1
Décollement
Barents Sea
NW
First thrust nappe
B
DE1
Glacier
Barents Sea
NW
Till deposition
A
Kanin ridge
Lacustrine and fluvial sediments
Shallow marine sediment
Barents Sea
Bedrock
Mud
Pre-deformation
20-40 km

Lab. No.	Sample No.	Site No.	Interbed	m a.s.l.	Age	± ka	Dose, Gy	± Gy	(n)	Dose rate, Gy/ka	± Gy/ka	w.c. %
021015	02-518	0209-53	1	5.9	114	9	165.53	10.68	11	1.45	0.06	28
021016	02-520	0209-53	1	11.4	183	13	126.91	5.19	11	0.69	0.04	26
021018	02-524	0209-53	1	12.8	188	22	157.3	16.64	10	0.84	0.04	25
001024	00-429	0007-3	1	6.5	129	14	270	25	20	2.09	n/d	14
001026	00-432	0007-25	1	28	111	12	220	20	20	1.99	n/d	27
001027	00-433	0007-25	1	37	149	10	284	8	26	1.91	n/d	27
021019	02-526	0209-55	2	19.5	136	10	190.43	11.21	24	1.4	0.06	26
021020	02-527	0209-55	2	20	119	9	160.85	9.85	21	1.35	0.05	32
021025	02-535	0209-158	2	23.8	92	6	150.05	7.28	35	1.63	0.06	32
001022	00-427	0007-7	2	43.3	158	13	247	13	18	1.56	n/d	24
001023	00-428	0007-7	2	36	117	10	235	15	21	2	n/d	18

Table 1

Lab.No.	Field No.	Site/ m from zero	m a.s.l.	Diam. Elem.	alle/Ile (HYD)	Average	St.dev.
BAL 3847 A	02-726	0209/550	35.0	DE4	0.025		
BAL 3847 B	02-726	0209/550	35.0	DE4	0.034		
BAL 3847 C	02-726	0209/550	35.0	DE4	0.036	0.032	0.006
BAL 3876	02-728	0209/550	34.0	DE4	0.037	0.037	
BAL 3879	02-744	0209/15500	63.0	DE3	0.032	0.032	
BAL 3846 A	02-736	0209/5400	29.0	DE2	0.025		
BAL 3846 B	02-736	0209/5400	29.0	DE2	0.032	0.029	0.005
BAL 3875 A	02-747	0210/7	11.0	DE2	0.097		
BAL 3875 B1	02-747	0210/7	11.0	DE2	0.085		
BAL 3875 B2	02-747	0210/7	11.0	DE2	0.081	0.088	0.008
BAL 3878	02-732	0209/5300	2.5	DE1	0.090	0.090	
BAL 3880	02-701	0209/1700	3.5	DE1	0.069	0.069	

Table 2